Tomographic inversion of time-domain resistivity and chargeability data for the investigation of landfills using a priori information

Giorgio De Donno*[1] and Ettore Cardarelli[1]

[1] *"Sapienza" University of Rome – DICEA Area Geofisica, Via Eudossiana 18, 00184 Rome, Italy*

*Corresponding author: giorgio.dedonno@uniroma1.it

Abstract

In this paper, we present a new code for the modelling and inversion of resistivity and chargeability data using a priori information to improve the accuracy of the reconstructed model for landfill. When a priori information is available in the study area, we can insert them by means of inequality constraints on the whole model or on a single layer or assigning weighting factors for enhancing anomalies elongated in the horizontal or vertical directions. However, when we have to face a multilayered scenario with numerous resistive to conductive transitions (the case of controlled landfills), the effective thickness of the layers can be biased. The presented code includes a model-tuning scheme, which is applied after the inversion of field data, where the inversion of the synthetic data is performed based on an initial guess, and the absolute difference between the field and synthetic inverted models is minimized.

The reliability of the proposed approach has been supported in two real-world examples; we were able to identify an unauthorized landfill and to reconstruct the geometrical and physical layout of an old waste dump. The combined analysis of the resistivity and chargeability (normalized) models help us to remove ambiguity due to the presence of the waste mass. Nevertheless, the presence of certain layers can remain hidden without using a priori information, as demonstrated by a comparison of the constrained inversion with a standard inversion. The robustness of the above-cited method (using a priori information in combination with model tuning) has been validated with the cross-section from the construction plans, where the reconstructed model is in agreement with the original design.

Keywords: electrical resistivity tomography, induced polarization, a priori information, landfill

1. Introduction

The detection and imaging of landfills are challenging tasks in geophysics, not only because of the required resolution and depth of penetration but also because major pitfalls may arise in such complex areas from the speculative interpretation of geophysical anomalies as geological or antrophic features (De Carlo et al., 2013). In particular, the latest national regulations (D.Lgs.

36/2003) were not everywhere adopted for the now covered landfill in Italy before 2003 and it could be difficult to reconstruct the effective succession of layers. Many landfills need prospecting for site management to assess the effective thickness of the different layers (e.g., compacted clay and saturated waste mass) and to verify the groundwater contamination due to leachate flow outside the landfill. In this sense, geophysical surveys can fulfil this target as long as they are able to investigate the whole landfill as constituted by anthropogenic (e.g., waste mass and leachate) and geological (e.g., clay and water table) features (Cardarelli and Bernabini, 1997). We can reconstruct the effective layering of the landfill to verify a possible leachate flow outside the site using geoelectrical methods, investigating both the resistive and the capacitive response of the waste mass (Gazoty et al., 2012). In fact, the waste layer is primarily depicted with a relatively high chargeable (> 10 mV/V) and conductive (< 2 Ωm) unit with respect to the surrounding media.

Electrical resistivity tomography (ERT) has been used worldwide for contaminant detection (e.g., Benson et al., 1997; Dahlin et al., 2002), investigation of landfills (e.g., Ogilvy et al., 2002; Cardarelli and Di Filippo, 2004; Chambers et al., 2006), and monitoring leachate injection (e.g., Audebert et al., 2016; Clément at al., 2010; 2011; Grellier et al., 2008) or DNAPLs source zones (e.g., Chambers et al., 2010; Power et al., 2014). ERT has also been employed in combination with induced polarization (IP) methods, where the acquisition is often performed in the time-domain for site monitoring (e.g., Ustra et al., 2012), monitoring of the DNAPLs plume (e.g., Cardarelli and Di Filippo, 2009), and classification of the contamination level (Turai, 2011). The added valued given by the joint analysis of the resistive and capacitive response of the subsoil has been demonstrated during last decades (e.g., Martinho and Almeida, 2006; Dahlin et al., 2010; Gazoty et al., 2012). In fact, the IP method is particularly sensitive to changes related to the presence of waste disposal or contamination (electrochemical polarisation), as well as changes in the clay content of geological formations (membrane polarisation).

The 2D and 3D inversions of ERT and IP datasets were frequently performed in literature by commercial software, such as RES2DINV/RES3DINV (Loke and Barker, 1996) or ERTLab (Geostudi Astier and Multiphase Technologies). Although these codes are rapid and reliable, they are closed-source programs, and the user cannot control the entire workflow or add new functions. Alternatively, open-source algorithms already available worldwide, such as BERT (Günther et al., 2006), RESINVM3D (Pilisecky et al., 2007), or EIDORS (Adler and Lionheart, 2006), perform almost only the inversion of ERT data, even though Karaoulis et al. (2013) recently developed a software in Matlab to perform ERT and IP inversion (IP4DI). In particular, EIDORS is a Matlab-based open-source software that was firstly developed for medical applications with the aim to share data and promote collaboration between groups working in this field. EIDORS is a well-

known package for electrical impedance tomography, generally performing a resistivity inversion on 3D cylindrically shaped domains with a linearised procedure. However, this code cannot be used in its current form to work on prismatic domains using a wider range of parameters (always for geophysical surveys). Moreover, an inversion code should take into account information coming from boreholes, direct inspection, and construction plans in the case of landfills to validate the inversion results. In the following sections we present a numerical code developed within the EIDORS environment, which is able to solve the 2D forward and inverse problems both for resistivity and chargeability and to embed a priori information within the numerical routines.

In addition, the effective thickness of the layers can be biased when we have to face a multilayered scenario with numerous resistive to conductive transitions (the case of landfills) and using ERT in combination with IP may be not sufficient to completely remove ambiguities in the interpretation of the inverted models. Therefore, the speculative interpretation of the inverted models is generally not adequate when we need to know the geometrical and physical layout of the landfill with a sufficient accuracy, and actions to remove these ambiguities should be adopted.

The main goals of this work are as follows:

- to evaluate the benefit of a priori information for the characterisation of landfills with a comparison between the standard approaches, where inversion is performed using a new code;
- to present a method for the ambiguity removal in the interpretation of landfill models by means of a model-tuning routine;
- to discuss the above-cited procedures with applications to real-world examples from the investigation of landfills.

2. Materials and Methods

2.1 Electrical parameters

The subsoil generally exhibits both a resistive and a capacitive response, where an external DC current source is turned on. The former effect can be modelled by means of the bulk resistivity (Archie, 1942):

$$\rho = \rho_w S^{-n} \Phi^{-m}, \quad (1)$$

where ρ_w is the solution resistivity, S is the degree of saturation, Φ is the porosity, and n and m are exponents depending on the tortuosity and cementation of the investigated medium.

The resistivity can be a diagnostic parameter for landfills because the high salinity of fluids often saturating the waste mass (leachate) usually makes them very conductive, in contrast to both the covering layer, often drier (Aristodemou and Thomas-Betts, 2000), and the bottom liner (HDPE)

that acts as an insulator (resistivity of 10^7 Ωm). However, if the waste mass is almost dry or inhomogeneous or if the clay constitutes a large fraction of the cover, it can be critical to distinguish the cover material from the waste (Ogilvy et al., 2002; Leroux et al., 2007). In addition, the identification of leaks is often unrealistic because the resistivity range of the clay bottom layer and the saturated waste are comparable (1–10 Ωm). To overcome these issues, we can also address the capacitive response of the subsurface in terms of chargeability, the ratio of the capacitive-to-conductive properties of the material at low frequencies (Slater and Lesmes, 2002). Chargeability is therefore linked to the changes in the bulk resistivity as it increases in the presence of a saline fluid (e.g., leachate), while no clear correlation is observed as a function of the clay content (Slater and Lesmes, 2002). Elsewhere in a landfill (covering, liners, dry waste), these parameters should be close to zero.

2.2 Code implementation

The theoretical formulation for solving the forward problem (Appendix A) and the inversion process (Appendix B) for resistivity and chargeability have been numerically implemented in Matlab using the VEMI algorithm—versatile algorithm for electrical modelling and inversion (De Donno and Cardarelli, 2015). This algorithm is capable to invert both time- and frequency-domain datasets acquired in the laboratory or in the field, and it is included in the open-source EIDORS environment. The choice of the piecewise path to be followed by the user is controlled in VEMI by the global variable *type* with four attributes*: domain* (time- or frequency-domain), *shape* (cylindrical for the laboratory or prismatic for the field survey, respectively), *geometry* (2D or 3D), and *inversion* (synthetic modelling or inversion), assuming values of 0/1 as a function of the particular choice. Each path is associated with the related functions for solving the forward and inverse problems (equations A.1–A.4 for 2D resistivity and chargeability modelling and B.1–B.5 for data inversion). Furthermore, versatile elements have been added to VEMI, which were specifically developed for landfills to reduce the degree of uncertainty in interpreting the geophysical models.

2.3 Versatile elements for landfills

2.3.1 Use of a priori information

When a priori information is available in the study area (e.g., we know length and thickness of the landfill layers), we can insert it in VEMI using inequality constraints on the new model vector **m'** (Kim et al., 1999):

$$\mathbf{m}' = \ln\left(\frac{\mathbf{m}-\mathbf{a}}{\mathbf{b}-\mathbf{m}}\right), \quad (1)$$

where **a** and **b** are vectors containing minimum and maximum acceptable values for the study parameter. This procedure can be applied both for the chargeability and resistivity model vectors, only within a particular sub-domain (e.g., the waste mass), or in the whole domain.

If information about the preferential direction of the anomalies is available, we can insert it by adding weights to the smoothness matrix in equation B.3, as:

$$\mathbf{L} = \alpha_x \mathbf{L_x} + \alpha_z \mathbf{L_z} , \quad (2)$$

where α_x and α_z are the weighting factors to enhance the anomalies elongated in the *x*- or *z*-directions. For a layered medium, $\alpha_z < \alpha_x$; for vertical anomalies $\alpha_z > \alpha_x$. For example, if we are investigating a landfill from its surface, we expect to address a horizontally elongated medium (e.g., unsaturated waste, saturated waste, and liner) and we can consider this information with a lower α_z/α_x ratio. On the contrary, if we aim to reconstruct a slurry wall, a higher α_z/α_x ratio would be assigned.

2.3.2 Normalised chargeability

A strategy to remove the ambiguity in the interpretation of electrical models can also be the separation of the IP effect due to the predominantly electrolytic control from effects due to clay content variation (Slater and Lesmes, 2002) through the normalisation of the chargeability. In fact, changes in clay content are clear in the response of but unclear in the response of. This effect can be relevant for landfills, where we need to discriminate between the two types of effects: IP structure resulting from electrolytic controls due to the waste mass and IP effect due to the clay layer often present underneath the bottom liner. The normalised chargeability mainly enhances the IP anomalies due to the increase in clay content; thus, we expect to have a higher in the correspondence to the clay soils and a relatively lower for the leachate. The normalised chargeability is given by the following:

$$\bar{\eta} = \eta/\rho , \quad (3)$$

where η and ρ are the chargeability and resistivity values inferred from the models inverted with VEMI.

2.3.3 Model tuning

The inverted geophysical section, although a reliable and low-error model, could be of non-univocal interpretation, referring to the effective thickness and depth of the detected interfaces. In fact, since the sensitivity (Jacobian matrix **J** in equation B.3) decreases substantially as a function of depth, any sharp variation occurring in the deeper zones cannot be followed by a rapid change in

resistivity. This effect can be clarified by mapping the sensitivities for each element *k* as a cumulative value as follows:

$$\mathbf{J}_{cum,k} = \frac{\sum_{q=1}^{N_Q} |\mathbf{J}_{q,k}|}{N_Q}, \quad (4)$$

where N_Q is the number of measurements and the absolute value of **J** is given to avoid situations, where a negative sensitivity value for one measurement cancels out the positive value for another measurement. An example of cumulative sensitivity is shown in Figure 1 for a homogeneous half-space of 10 Ωm investigated using 48 electrodes spaced 5 m apart using a pole–dipole array with a_{max} = 5 and n_{max} = 6. This equation clearly demonstrates that the deeper the target to be resolved is, the lower are the sensitivity to the resistivity changes and consequently the resolution of the anomalies. Owing to the above considerations, a further iterative procedure can give a quantitative estimation of the landfill model (Fig. 2). Starting from an initial guess for the landfill model derived from the inversion of field data, we perform the synthetic simulation and the subsequent inversion of the synthetic dataset. We can finally estimate the landfill model using the iterative minimisation of the absolute difference between the field and synthetic final models. This procedure is similar to that proposed by Narayan et al. (1994).

In the following sections, we present the application of the above-cited procedures to real-world examples.

2.4 Study sites

2.4.1 RW01 - Unauthorized landfill (Lazio region, Italy)

Location

The site, located 10 km from Rome, is an old tuff quarry covered with backfill and waste since the 1990s. The unauthorized waste disposal was suspected by the local authority because of the contamination of the neighbouring creeks, even if they actually ignored the effective depth of the bedrock and the typology of the buried waste. The tuff deposits, partially emerging in the elevated NW part of the area, have probably been excavated up to 20 m from the former surface. Geophysical investigations aim to detect the tuff bedrock and to assess if the site could be a landfill.

Geophysical measurements

Three 2D ERT lines were performed in the area: L1, entirely located within the supposed landfill; L2, partially covering the outcropping bedrock; and L3, outside the landfill towards the direction of the groundwater flow (Fig. 3). The ERT lines employed 48 stainless steel electrodes spaced 3 m apart using the resistivimeter Syscal Pro 48 electrodes produced by Iris Instruments with a pole–

dipole array. The pole–dipole array using both forward and reverse schemes (Clément at al., 2010) has been employed for each line with one current electrode theoretically placed at an infinite distance from the other current electrode (in this case, at 1000 m parallel to the line) and is able to reach a sufficient depth of investigation without losing resolution. The customised sequence of acquisition has been generated with a maximum electrode separation a_{max} = 5 and a dipole separation factor n_{max} = 6, resulting in 1035 measurements for each dataset. The chargeability dataset was acquired using an injection pulse duration of 1 s and semi-logarithmic sampling of the decay curve (20 gates). The latter parameters have been chosen subsequent to a preliminary trial with different pulse durations and numbers of gates. These parameters allow good sampling of the decay curve without a drastic increase of the acquisition time.

Although the use of non-polarisable electrodes for the chargeability is the optimum choice, reliable measurements can be acquired by employing steel electrodes (La Brecque and Daily, 2008; De Donno and Cardarelli, 2011), as in this case.

2.4.2 RW02 - Authorised landfill (Lazio region, Italy)

Location

The investigated area, located in the Lazio region, is a landfill built in the 1990s as part of a bigger complex for using as waste disposal of a medium-sized city. The site was provided with a bottom liner (geo-membrane and compacted clay) and it had been active for ten years until it was covered. Geophysical investigations have been planned for the site management to evaluate the effective depth of the bottom liner and to verify a possible leachate flow outside the site.

The geological setting of the surrounding area is mainly characterised by pyroclastic shallow deposits overlying a clay horizon and sand. Boreholes drilled in the surrounding area indicate that the interface between the clay and sand should be located approximately 25 m from the surface.

Geophysical measurements

The geophysical campaign had to preliminarily take into account the supposed depth of the buried waste (low-permeability layers), the resolution needed, and costs. For this reason, four electrical lines spaced 30 m apart (L1 to L4) and employing 48 electrode spaced 5 m apart (Fig. 4) were performed with the resistivimeter Syscal Pro 48 using a pole–dipole array and the same acquisition parameters as in RW01.

3. Results

In the following sections, we present the results of the inverted models, a comparison with the standard approach, and the added value given by the model-tuning procedure.

3.1 RW01

The results of the 2D inversions are shown in Figure 5 for the resistivity and in Figure 6 for the chargeability dataset. Because there is no a priori information available for this site linked to the thickness or the length of the waste disposal, we set without using inequality constraints.

The inverted models display low RMSE values at the final iteration, always below 5% for resistivity and 2 mV/V for chargeability.

The L1 model (Figs 5a and 6a) shows low-resistivity values in correspondence with a high capacitive response probably related to the waste mass. The resistivity values of the model range from 1 to 60–70 Ωm, except for the shallower layer (probably backfill), where ρ reaches values up to 100 Ωm. This evidence is confirmed by the L2 models (Figs. 5b and 6b), which explain the excavated tuff deposits (up to 20 m) emerging in the NW part of the site. The high resistivity values are associated with the tuff deposits, while the conductive overlying layer is related to the waste mass. The resistivity model alone (Fig. 5b) is not sufficient to infer, with an acceptable accuracy, that the conductive layer belongs to a waste mass. The nature of the layer is clarified when the resistivity and chargeability models are analysed jointly: the conductive area corresponds to high chargeability values. The L3 resistivity model (Fig. 5c) shows a similar behaviour with respect to L2 (Fig. 5b), even though there is no visible chargeable anomaly in this model (Fig. 6c). Therefore, we can confirm that the old tuff quarry was used as a waste disposal, the waste mass extended up to 20 from the surface, and no significant anomaly was found in the direction of the groundwater flow. The waste mass is covered by backfill in the shallower 2 m.

3.2 RW02

The inverted models are reported in Figures 7 and 8 for resistivity and chargeability, respectively. For the RW02 case we set a layered medium with anomalies elongated in the horizontal direction because we expect controlled landfill from the surface. The resistivity model was forced to vary only within the expected 0.5–200-Ωm range for the landfill and the *in situ* deposits using inequality constraints on the resistivity model. The values were set with reference to the commonly known ranges for the clay and sandy deposits in the study area and for the anthropogenic elements (waste, leachate).

The four models still present low RMSE values, even though $RMSE_\eta$ is slightly higher due to an increasing level of noise. The resistivity models (Fig. 7) are homogeneous among themselves, with

similar layering and resistivity values. We detect a shallow resistive layer (z = 0–8 m, ρ = 40 Ωm) related to the covering and the unsaturated waste that overlies a high-conductive target (z = 8–15 m, ρ = 1 Ωm). This layer is confined at the right, left and bottom sides by a slightly resistive layer, which may be related to the bottom liner (z = 15–20 m, ρ = 40 Ωm). This layer is detected at z = 10–15 m of the L4 line (Fig. 7a), executed approximately 3 m lower, close to the edge of the landfill, where we expect the bottom liner to be shallower. The conductive and resistive layers located in the deep can be attributed to the *in situ* clay and sand deposits, respectively. However, although the recovered layering could be consistent with that expected for this landfill, we cannot deduce the thickness and the resistivity values with an adequate degree of accuracy due to multiple successions of conductive and resistive units.

The chargeability models (Fig. 8) are more heterogeneous; we are not able to determine a definite correspondence between the resistivity and chargeability anomalies. In fact, high chargeability values are displayed not only in correspondence to the shallower conductive layer but also to the bottom part of the sections. However, we cannot identify if the deeper chargeable anomalies are due to the clay deposits (membrane polarisation) or to the presence of a leachate flow outside the landfill.

3.2.1 Normalised chargeability

The added value given by the normalised chargeability is illustrated in Figure 9, with reference to the RW02 case study. We can discriminate two clear chargeable anomalies due to the waste mass (shallower, from 8 to 12 m) and increasing clay content (deeper, from 20 to 45 m, variable as a function of the ERT line); we correlate these models with the resistivity anomalies (Fig. 7), where the conductive layers correspond to the chargeable layers. The normalised chargeability related to an increase in the clay content is higher than that pertinent to the waste mass according to previous results (Slater and Lesmes 2002).

3.3 Comparison with standard approaches

The results from the standard inversion performed without using inequality constraints and weighting factors are presented in Figures 10a and 10c (software RES2DINV) and in Figures 10b and 10d (software VEMI) for the L3 line of the RW02 case study. The resistivity models are characterised by higher RMSE values (13–15 %); the separation between the landfill and the *in situ* deposits is not visible and consequently these sections are not representative for the effective layering.

3.4 Model tuning

The routine described in 2.2.3 was applied to the L3 line of RW02. A zero mean Gaussian noise was added separately to the resistivity and chargeability datasets, with standard deviation levels set to 3% and 1 mV/V, respectively. The final models are represented in Figure 11 together with the inverted models of the synthetic data of the last iteration. The models are composed of a resistive top layer (corresponding to covering and dry waste), a highly conductive and chargeable thin layer (waste mass saturated by leachate), and a resistive layer (bottom liner and drains). The maximum depth of the landfill is 12.5 m. The interface between the *in situ* clay and sand is located at 25 m (Fig. 11). The comparison between the inverted models from real (Figs 7c and 9c) and synthetic data (Figs. 11c and 11d) provides a quantitative estimation of the error in terms of absolute differences between the two models (Fig. 12). This section displays values below 20 Ωm, except in the correspondence with boundaries and near the surface, where the degree of heterogeneity is higher. We choose the best fit from a direct inspection of the absolute difference section and use it as the estimate for the landfill model changes. Although the automatic minimisation of the absolute difference between the two models is recommended from a theoretical point of view, it practically requires the introduction of an outer iterative routine that corresponds to a non-linear increase of the computational time. In addition, we always need to direct the comparison between the field and synthetic model toward the achievement of a physically based landfill model, where geometry and resistivity values are in agreement with the commonly used geometries and materials employed because the final model should be simple, informative, and not only the result of a mere mathematical optimization**.**

4. Discussion

The comparison between the final electrical mode of line L3 and the correspondent cross-section from the construction plans of the landfill (A-A' in Fig. 4) is plotted in Figure 13. The two major discontinuities (waste-clay and clay-sand) were detected at the same depth of the original design (12.5 and 25 m), while the geophysical model differs only for x > 200 m, where we assume terraces for drainage that differ from the original design. Therefore, the constrained inversion of the geophysical data, with the reconstructed models tuned later through a comparison with synthetic data, returns a landfill model comparable with the true one both for thickness and length of the different layers. The comparison of the results from model tuning (Fig. 11c) with those achieved by standard inversion (Fig. 10a, RES2DINV, and Fig. 10b, VEMI) clearly demonstrates that we can derive the effective layering of the landfill (5 layers) only using a priori information. In particular, the bottom liner is correctly identified at the proper depth (12 m). On the contrary, we are able to

identify only 3 layers (resistive, conductive, resistive) through standard inversion and the effective depth of the landfill is strongly biased (> 40 m).

As an alternative and given a priori construction plans, users could perform a constrained inversion assigning inequality constrains for each layer (waste and *in situ* deposits) to steer the inversion process toward the effective layering. Using this procedure without performing the model tuning implies the knowledge of the thickness of the saturated waste from direct inspection. In addition, the leachate could undergo noteworthy temperature changes reflected in the resistivity and high variability of the chargeability, which should be considered for the proper setting of the **a** and **b** vectors (minimum and maximum acceptable values for inequality constraints). However, the importance of a priori information in the inversion process can be evaluated comparing the models of RW02-L3 shown in Figures 7c and 9c (constrained inversion with VEMI) and in Figure 10 (standard inversion with RES2DINV and VEMI). The multilayer behaviour of the landfill is revealed only using a priori information in combination with model tuning recovering lower RMSE values (for resistivity) compared to the standard inversion (3% vs. 13%).

Moreover, the presence of the geomembrane could create distortions in the electrical field, as demonstrated by Audebert et al. (2014) for Wenner-Schlumberger, dipole-dipole, and gradient arrays and a finite boundary condition should be inserted to model the effect of the bottom liner acting as an insulator. In this case, the pole-dipole array, which was not investigated in this sense, yet, has given reliable results without considering a finite boundary condition, as confirmed by the validation of the models. Further improvement should concern the investigation of the geomembrane effect for this configuration. We stress the importance of acquiring consistent datasets (sum of quality of instrumentation, electrodes, and array choice), which is a pivotal issue for ERT and IP investigations. The data quality of the inversion process is much more important than that of other inversion parameters, as demonstrated by the higher RMSE values of the RW02 models, where the datasets are affected by a higher level of noise.

The results from the RW01 case study (L2) demonstrate that the standard inversion procedure could also be acceptable in the case of uncontrolled or unauthorized landfill (widespread in Italy), whereas we generally have a simple two-layer model (conductive-waste mass; resistive-bedrock). Because the normalised chargeability is highly sensitive to changes in the clay content for investigations of controlled landfills in Italy after 2003, where a low-permeability clayey formation is always present, as stated in previous work (Dahlin et al., 2010; Ustra et al., 2012), the numerical codes should include the comparison between the normalised and raw parameters to understand the mechanism of polarisation associated with the different anomalies.

Conclusions

In this paper, we demonstrated the added value given by the use of a priori information for landfill characterisation. This information can be utilised by means of inequality constraints within our numerical algorithm, limiting the range of variation of the selected parameters within a certain area (the whole model or a single layer), or using weighting factors of the smoothness matrix to enhance anomalies elongated in the horizontal (where the survey is performed from the top of the landfill) or vertical (for surveys on slurry walls). Where inversion is accomplished, users can improve the results with a model tuning procedure. This procedure consists of a further iterative loop in which the inversion of synthetic data is performed starting from an initial guess and the absolute difference between the field and synthetic inverted models is minimized. When convergence is reached, the landfill model and the synthetic model of the last iteration are consistent.

The reliability of this approach has been demonstrated in two field examples of different scenarios: the detection of an unauthorised landfill and the geometrical and physical characterisation of an old authorised landfill. The final inverted models display low-RMSE values both for resistivity (below 5%) and chargeability (below 2 mV/V), except for the RW02 chargeability dataset affected by a higher level of noise (maximum value of 8 mV/V). The role the chargeability played in removing the ambiguity of the resistivity models was stressed in this paper; we are not able to discern the waste mass by only looking at the resistivity model. We can argue with a sufficient degree of confidence that the investigated subsoil is contaminated or is a landfill when the conductive anomalies correspond to the chargeable zones. However, in cases where electrochemical and membrane IP effects overlap (RW02), the chargeability models are not diagnostic, and the use of the normalised chargeability can help to increase consequently the degree of accuracy in landfill reconstruction.

We reconstructed the geometrical and physical layering of the subsoil for the RW02 case using a priori information and the model tuning routine, providing a quantitative model of the old landfill. In fact, the use of inequality constraints or weighting factors of the smoothness matrix can help to improve the resolution of the inverted models in complex scenarios with multiple successions of conductive and resistive layers (the case of controlled landfills). Some layers cannot be noted without using these parameters, as proven by a comparison with a standard inversion performed with VEMI and RES2DINV (widespread use for the inversion of ERT/IP data). The robustness of the above-cited method (using a priori information in combination with model tuning) has been confirmed through a comparison with the cross-section from the construction plans, where the reconstructed model is in agreement with the original design.

This procedure requires further improvement concerning the development of an automatic routine to identify the optimum model through the minimisation of the absolute difference between the inverted models of the synthetic and field datasets. Future work should concern the application of a priori information with VEMI to complex resistivity tomography, including the acquisition of frequency-domain data on RW01 and/or RW02, to compare between time-domain and frequency-domain datasets for the investigation of landfills.

Appendix A. Forward modelling

The resistive response of a subsoil *D* can be defined by the following equation, where electrodes are modelled as points (point electrode model – PEM) and the conductivity is assumed invariant along the y-direction (e.g., Dey and Morrison, 1979; Queralt et al., 1991; Cardarelli and Fischanger 2006):

$$-\nabla \cdot \left[\sigma(x,z)\nabla\tilde{\phi}(x,z,\lambda)\right] + \lambda^2\sigma(x,z)\tilde{\phi}(x,z,\lambda) = 0.5I\delta(x_S)\delta(z_S)\,, \quad \text{(A.1)}$$

where σ is the conductivity (ρ=1/σ is the resistivity), $\tilde{\phi}$ is the transformed electric potential, λ is the transformed variable, and I is the injected current.

Equation (1) is subject to the following boundary conditions:

$$\sigma\frac{\partial\tilde{\phi}}{\partial\nu} = 0 \; on \; D_S \; ; \frac{\partial\tilde{\phi}}{\partial\nu} + \frac{\tilde{\phi}cos\theta}{R} = 0 \; on \; D_\infty \quad \text{(A.2)}$$

where D_S is the surface, D_∞ are the lateral and bottom boundaries located "far enough" from the source, and θ is the angle between the radial distance *R* and the outward normal ν. This formulation is often called the 2.5D approximation.

Many numerical approaches have been adopted to the solution of (A.1) and (A.2) during the last decades, both using the finite element method (Pridmore et al., 1981) and the finite difference method (Dey and Morrison, 1979). A widely used technique is the Galërkin formulation of the finite element method (e.g., Vauhkonen 1997; Bastos and Sadowski 2003; Rücker and Günther 2011).

Once the solution of (1) and (2) is achieved, the predicted apparent resistivity is given by:

$${\rho_a}^{pre} = K\frac{\Delta\phi}{I}\,, \quad \text{(A.3)}$$

where *K* is the geometric factor and $\Delta\phi$ is obtained according to the particular sequence of the measurements.

The effect of the chargeability is modelled using the same resistivity forward mapping (Eqs. A.1–A.2) but with the conductivity replaced by $\sigma(1-\eta)$ (Siegel, 1959; Oldenburg and Li, 1994). The predicted apparent chargeability is defined as:

$${\eta_a}^{pre} = \frac{\phi_\eta - \phi_\sigma}{\phi_\eta}\,, \quad \text{(A.4)}$$

where ϕ_η and ϕ_σ are the potential resulting from the forward solutions for chargeability and conductivity, respectively.

Appendix B. Inversion

The resistive behaviour of a subsoil is generally measured in the time-domain as apparent resistivity ρ_a, while the capacitive response is measured as apparent chargeability η_a:

$$\rho_a{}^{obs} = K\frac{V_p}{I}, \tag{B.1}$$

$$\eta_a{}^{obs} = \frac{\int_{ti}^{tf} V_i dt}{V_p \Delta t}, \tag{B.2}$$

where V_p is the measured voltage during the application of the current I and V_i is the residual voltage after the termination of an applied current integrated over a time window Δt defined between times t_i and t_f.

We employed a Gauss–Newton iterative formulation to invert the apparent resistivity data, where the optimum damping factor is chosen for each outer iteration h as the value that minimises the RMSE (De Donno, 2013):

$$\delta\mathbf{m}_h = [\mathbf{J}(\mathbf{m}_h)^{\mathrm{T}}\mathbf{W}^{\mathrm{T}}\mathbf{W}\,\mathbf{J}(\mathbf{m}_h) + \alpha_h\mathbf{L}^{\mathrm{T}}\mathbf{L}]^{-1}\cdot\{\mathbf{J}(\mathbf{m}_h)^{\mathrm{T}}\mathbf{W}^{\mathrm{T}}\mathbf{W}[\mathbf{d} - g(\mathbf{m}_h)] - \alpha_h\mathbf{L}^{\mathrm{T}}\mathbf{L}(\mathbf{m}_h - \mathbf{m}_0)\}, \tag{B.3}$$

where $\mathbf{m} = \ln(\boldsymbol{\rho})$ is the model update vector, $\mathbf{J}$ is the Jacobian matrix ($J_{q,k} = \frac{\partial d_q}{\partial m_k}$), $\mathbf{W} = diag(\frac{1}{\boldsymbol{s^\rho}/100})$ is the data weight matrix ($\boldsymbol{s^\rho}$ is the observed standard deviation vector expressed in %), α is the damping factor, $\mathbf{L}$ is the smoothness matrix (Tsourlos and Ogilvy, 1999), $\mathbf{d} = \ln(\boldsymbol{\rho_a}^{obs})$ is the observed data vector, $g(\mathbf{m}) = \ln(\boldsymbol{\rho_a}^{pre})$ is the predicted data vector, h is the outer iteration, and q is the measured quadrupole.

The chargeability dataset is inverted following the procedure described in Oldenburg and Li (1994) as method III, which is a nonlinear sequential inversion of resistivity and chargeability data. Once the resistivity model has been recovered through (B.3), we perform another inversion routine with the following substitutions:

$$\mathbf{d} = \ln(\boldsymbol{\eta_a}^{obs});\ g(\mathbf{m}) = \ln(\boldsymbol{\eta_a}^{pre});\ \mathbf{m} = \boldsymbol{\eta};\ \mathbf{W} = diag(\frac{1}{\boldsymbol{s^\eta}/1000}), \tag{B.4}$$

where $\boldsymbol{s^\eta}$ is the observed standard deviation expressed in mV/V.

The iterative procedure is stopped when the root mean square error (RMSE) is acceptable for the resistivity and chargeability dataset, as follows:

$$RMSE_\rho = \sqrt{\frac{\sum_{q=1}^{N_Q}\left(\frac{\rho_{a\,q}^{obs} - \rho_{a\,q}^{pre}}{\frac{s_q^\rho}{100}\rho_{a\,q}^{obs}}\right)^2}{N_Q}};\ RMSE_\eta = \sqrt{\frac{\sum_{q=1}^{N_Q}\left(\frac{\eta_{a\,q}^{obs} - \eta_{a\,q}^{pre}}{\frac{s_q^\eta}{1000}}\right)^2}{N_Q}}, \tag{B.5}$$

where N_Q is the number of measurements.

Because the chargeability values are often close to zero (few mV/V), the choice of an absolute value for RMSE is convenient and more diagnostic (De Donno and Cardarelli, 2014). Convergence is reached when the RMSE difference between two consecutive iterations (*h* and *h*-1) is lower than 1%.

Acknowledgements

This research was funded by the Department of Civil, Constructional and Environmental Engineering of "Sapienza" University of Rome - Grant 2015.

References

Adler, A. and Lionheart, W. 2006. Uses and abuses of EIDORS: An extensible software base for EIT. Physiological Measurement 27, 25–42.

Aristodemou, E. and Thomas-Betts, A. 2000. DC resistivity and induced polarisation investigations at a waste disposal site and its environments. Journal of Applied Geophysics 44(2), 275-302.

Audebert, M., Clément, R., Grossin-Debattista, J., Günther, T., Touze-Foltz, N. and Moreau, S. 2014. Influence of the geomembrane on time-lapse ERT measurements for leachate injection monitoring. Waste Management 34(4), 780-790.

Audebert, M., Oxarango, L., Duquennoi, C., Touze-Foltz, N., Forquet, N. and Clément, R. 2016. Understanding leachate flow in municipal solid waste landfills by combining time-lapse ERT and subsurface flow modelling–Part I: Analysis of infiltration shape on two different waste deposit cells. Waste Management (in press), doi:10.1016/j.wasman.2016.04.006

Bastos, J.P.A. and Sadowski, N. 2003. Electromagnetic modeling by Finite Element Method. Marcel Dekker, New York, Electrical Engineering and Electronic Series, Vol. 117, ISBN: 0-8247-4269-9.

Benson, A. K., Payne, K.L. and Stubben, M.A. 1997. Mapping groundwater contamination using dc resistivity and VLF geophysical methods-A case study. Geophysics 62(1), 80-86.

Cardarelli, E. Bernabini, M. 1997. Two case studies of the determination of parameters of two urban waste dumps. Journal of Applied Geophysics 36, 167-174

Cardarelli, E. and Di Filippo, G. 2004. Integrated Geophysical Survey on waste dumps: evaluation of physical parameters to characterize an urban waste dump (Four case studies in Italy). Waste Management & Research 22, 390-402

Cardarelli, E. and Di Filippo, G. 2009. Electrical resistivity and induced polarization tomography in identifying the plume of chlorinated hydrocarbons in sedimentary formation: a case study in Rho (Milan-Italy). Waste Management & Research 27, 595-602.

Cardarelli, E. and Fischanger, F. 2006. 2D data modelling by electrical resistivity tomography for complex subsurface geology. Geophysical Prospecting 54, 121–133.

Chambers, J.E., Kuras, O., Meldrum, P.I., Ogilvy, R.D. and Hollands, J. 2006. Electrical resistivity tomography applied to geologic, hydrogeologic, and engineering investigations at a former waste-disposal site. Geophysics 71(6), B231-B239.

Chambers, J.E., Wilkinson, P.B., Wealthall, G. P., Loke, M.H., Dearden, R., Wilson, R. and Ogilvy, R.D. 2010. Hydrogeophysical imaging of deposit heterogeneity and groundwater chemistry changes during DNAPL source zone bioremediation. Journal of Contaminant Hydrology 118(1), 43-61.

Clément, R., Descloitres, M., Günther, T., Oxarango, L., Morra, C., Laurent, J. P. and Gourc, J.P. 2010. Improvement of electrical resistivity tomography for leachate injection monitoring. Waste Management 30(3), 452-464.

Clément, R., Oxarango, L. and Descloitres, M. 2011. Contribution of 3-D time-lapse ERT to the study of leachate recirculation in a landfill. Waste Management 31(3), 457-467.

Dahlin, T., Bernstone, C. and Loke, M.H. 2002. A 3-D resistivity investigation of a contaminated site at Lernacken, Sweden. Geophysics 67(6), 1692-1700.

Dahlin, T., Rosqvist, H. and Leroux, V. 2010. Resistivity-IP mapping for landfill applications. First Break 28(8), 101-105.

De Carlo, L., Perri, M.T., Caputo, M.C., Deiana, R., Vurro, M. and Cassiani, G. 2013. Characterization of a dismissed landfill via electrical resistivity tomography and mise-à-la-masse method. Journal of Applied Geophysics 98, 1-10.

De Donno, G. and Cardarelli, E., 2011. Assessment of errors from different electrode materials and configurations for electrical resistivity and time-domain IP data on laboratory models. Bollettino di Geofisica Teorica e Applicata 52, 211–223.

De Donno, G. 2013. 2D tomographic inversion of complex resistivity data on cylindrical models. Geophysical Prospecting 61(Suppl.1), 586–601.

De Donno, G. and Cardarelli, E. 2014. 3D complex resistivity tomography on cylindrical models using EIDORS. Near Surface Geophysics 12(5), 587-598.

De Donno, G. and Cardarelli, E. 2015. A Flexible Interface for Tomographic Inversion of Real and Complex Resistivity Data in EIDORS. 21th European Meeting of Environmental and Engineering Geophysics, Turin, Italy.

533 Dey, A. and Morrison, H.F. 1979. Resistivity modelling for arbitrarily shaped two-dimensional
534 structures. Geophysical Prospecting 27, 106–136.
535 Gazoty, A., Fiandaca, G., Pedersen, J., Auken, E., Christiansen, A.V. and Pedersen, J.K. 2012.
536 Application of time domain induced polarization to the mapping of lithotypes in a landfill site.
537 Hydrology and Earth System Sciences 16(6), 1793-1804.
538 Grellier, S., Guérin, R., Robain, H., Bobachev, A., Vermeersch, F. and Tabbagh, A. 2008.
539 Monitoring of leachate recirculation in a bioreactor landfill by 2-D electrical resistivity imaging.
540 Journal of Environmental & Engineering Geophysics 13(4), 351-359.
541 Günther, T., Rücker, C. and Spitzer, K. 2006. Three-dimensional modelling and inversion of
542 dc resistivity data incorporating topography — II. Inversion. Geophysical Journal International
543 166(2), 506–517.
544 Karaoulis, M., Revil, A., Tsourlos, P., Werkema, D.D. and Minsley, B.J. 2013. IP4DI: A software
545 for time-lapse 2D/3D DC-resistivity and induced polarization tomography. Computers &
546 Geosciences 54, 164-170.
547 Kim, H.J., Song, Y. and Lee, K.H. 1999. Inequality constraint in least squares inversion of
548 geophysical data. Earth Planets Space 51, 255–259.
549 La Brecque, D.J. and Daily, W. 2008. Assessment of measurement errors for galvanic-resistivity
550 electrodes of different composition. Geophysics 73, 55-64.
551 Leroux, V., Dahlin, T. and Svensson, M. 2007. Dense resistivity and induced polarization
552 profiling for a landfill restoration project at Härlöv, Southern Sweden. Waste Management &
553 Research 25(1), 49-60.
554 Loke, M.H. and Barker, R.D. 1996. Rapid least squares inversion of apparent resistivity
555 pseudosections by a quasi- Newton method. Geophysical Prospecting 44, 131-152.
556 Martinho, E. and Almeida, F. 2006. 3D behaviour of contamination in landfill sites using 2D
557 resistivity/IP imaging: case studies in Portugal. Environmental Geology 49(7), 1071-1078.
558 Narayan, S., Dusseault, M.B. and Nobes, D.C. 1994. Inversion techniques applied to resistivity
559 inverse problems. Inverse Problems 10(3), 669.
560 Ogilvy, R., Meldrum, P., Chambers, J., and Williams, G. 2002. The use of 3D electrical resistivity
561 tomography to characterise waste and leachate distribution within a closed landfill, Thriplow, UK.
562 Journal of Environmental & Engineering Geophysics 7(1), 11-18.
563 Oldenburg, D.W. and Li, Y. 1994. Inversion of induced polarization data. Geophysics 59, 1327-
564 1341.
565 Pidlisecky, A., Haber, E. and Knight, R. 2007. RESINVM3D: A 3D resistivity inversion package.
566 Geophysics 72(2), H1-H10.

Power, C., Gerhard, J.I., Karaoulis, M., Tsourlos, P. and Giannopoulos, A. 2014. Evaluating four-dimensional time-lapse electrical resistivity tomography for monitoring DNAPL source zone remediation. Journal of Contaminant Hydrology 162, 27-46.

Pridmore, D., Hohmann, G.W., Ward, S.H. and Sill, W. 1981. An investigation of finite element modeling for electrical and electromagnetic data in three dimensions. Geophysics 46, 1009-1024.

Queralt, P., Pous, J. and Marcuello, A. 1991. 2-D resistivity modeling: an approach to arrays parallel to the strike direction. Geophysics 56, 941–950.

Rücker, C. and Günther, T. 2011. The simulation of finite ERT electrodes using the complete electrode model. Geophysics 76, F227–F238.

Seigel, H.O. 1959. Mathematical Formulation and Type Curves for Induced Polarization, Geophysics 24, 3, 547-565.

Slater, L.D. and Lesmes, D. 2002. IP interpretation in environmental investigations. Geophysics 67, 77-88.

Tsourlos, P. and Ogilvy, R. 1999. An algorithm for the 3-D Inversion of Tomographic Resistivity and Induced Polarisation data: Preliminary Results. Journal of the Balkan Geophysical Society 2, 30–45.

Turai, E. 2011. Data processing method developments using TAU-transformation of Time-Domain IP data. II. Interpretation results of field measured data. Acta Geodaetica et Geophysica Hungarica, 46(4), 391-400.

Ustra, A.T., Elis, V.R., Mondelli, G., Zuquette, L.V. and Giacheti, H.L. 2012. Case study: a 3D resistivity and induced polarization imaging from downstream a waste disposal site in Brazil. Environmental Earth Sciences 66(3), 763-772.

Vaukhonen, M. 1997. Electrical impedance tomography and prior information. PhD Thesis, Department of Applied Physics, Kuopio University, Finland.

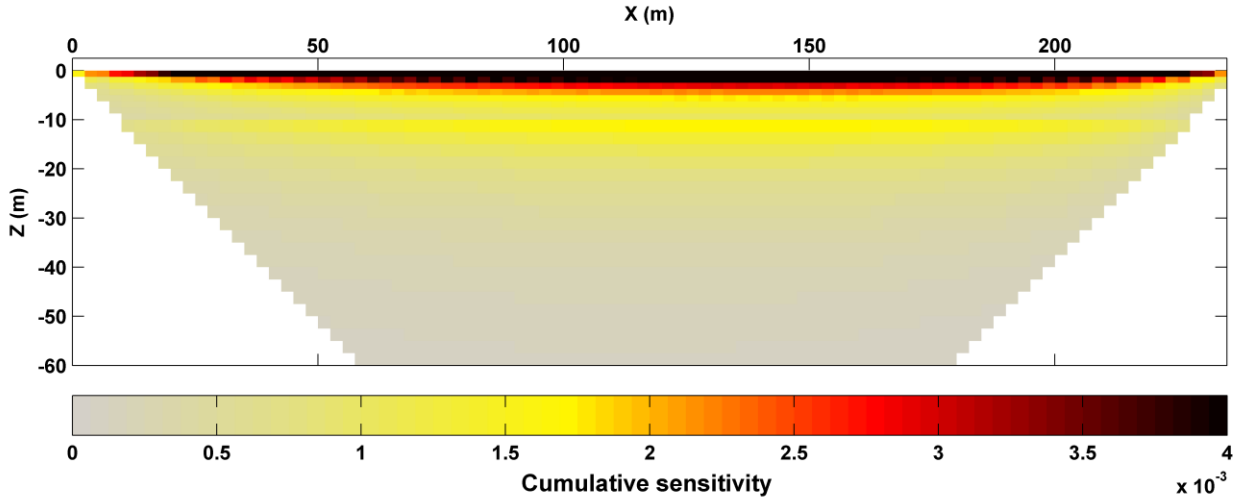

591

592 Figure 1. Example of cumulative sensitivity for an homogeneous half-space (10 Ωm) investigated
593 using 48 electrodes spaced 5 m apart using a pole-dipole array with a_{max} = 5 and n_{max} = 6.

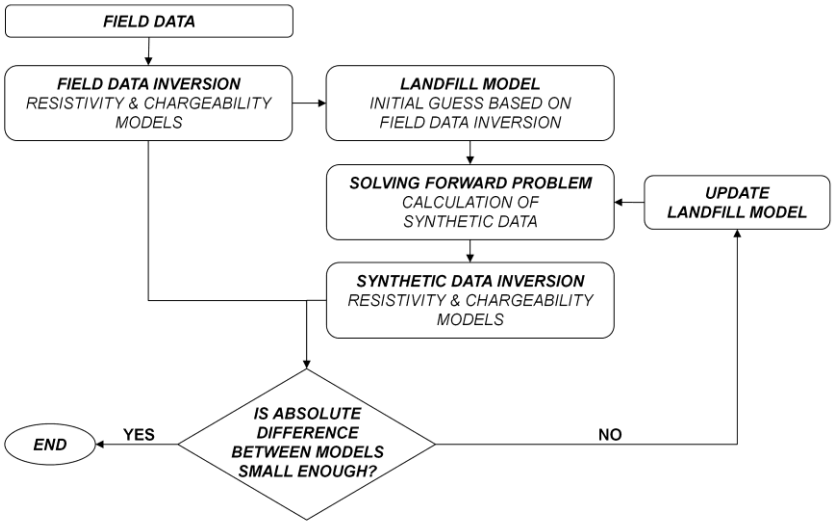

594

595 Figure 2. Flow-chart of the model tuning procedure to find the optimum landfill model.

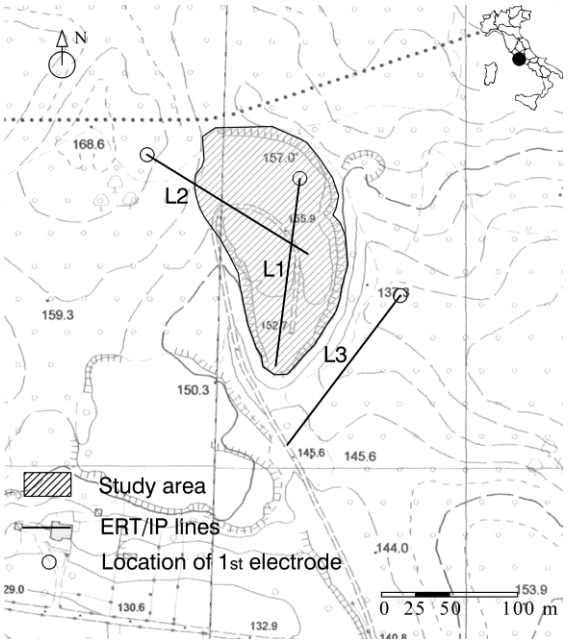

596

597 Figure 3. Topographic plan of the RW01 site with the location of the ERT/IP lines.

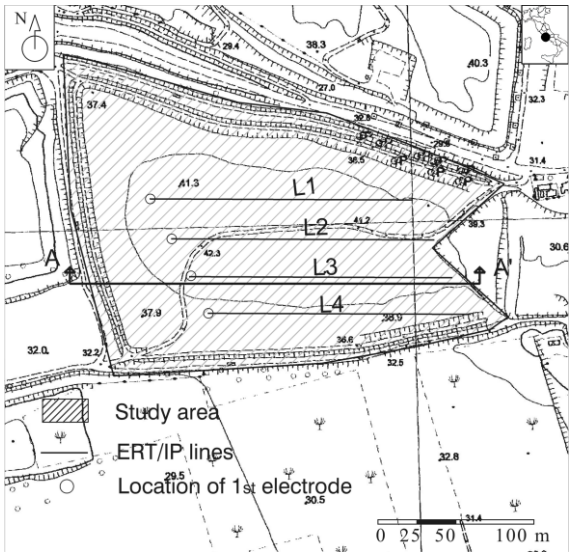

598

599 Figure 4. Topographic plan of the RW02 site with the location of the ERT/IP lines and of the A-A'
600 section from the construction plans.

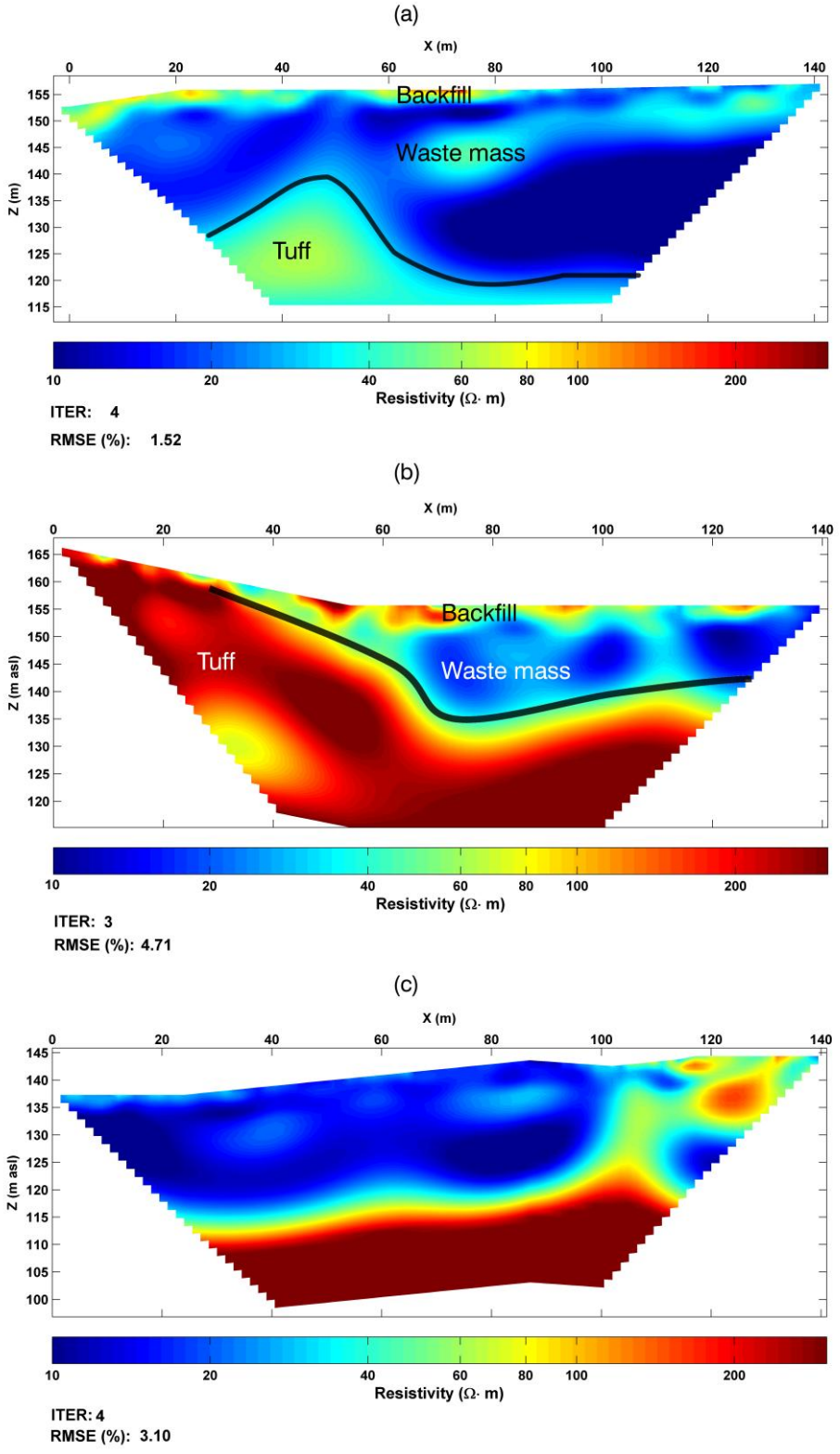

Figure 5. Resistivity inverted models of ERT/IP L1 (a), L2 (b) and L3 (c) lines for the RW01 site. The direction of the line and the position of the first electrode are shown in Fig. 3. The black lines indicate the interface between waste mass and tuff.

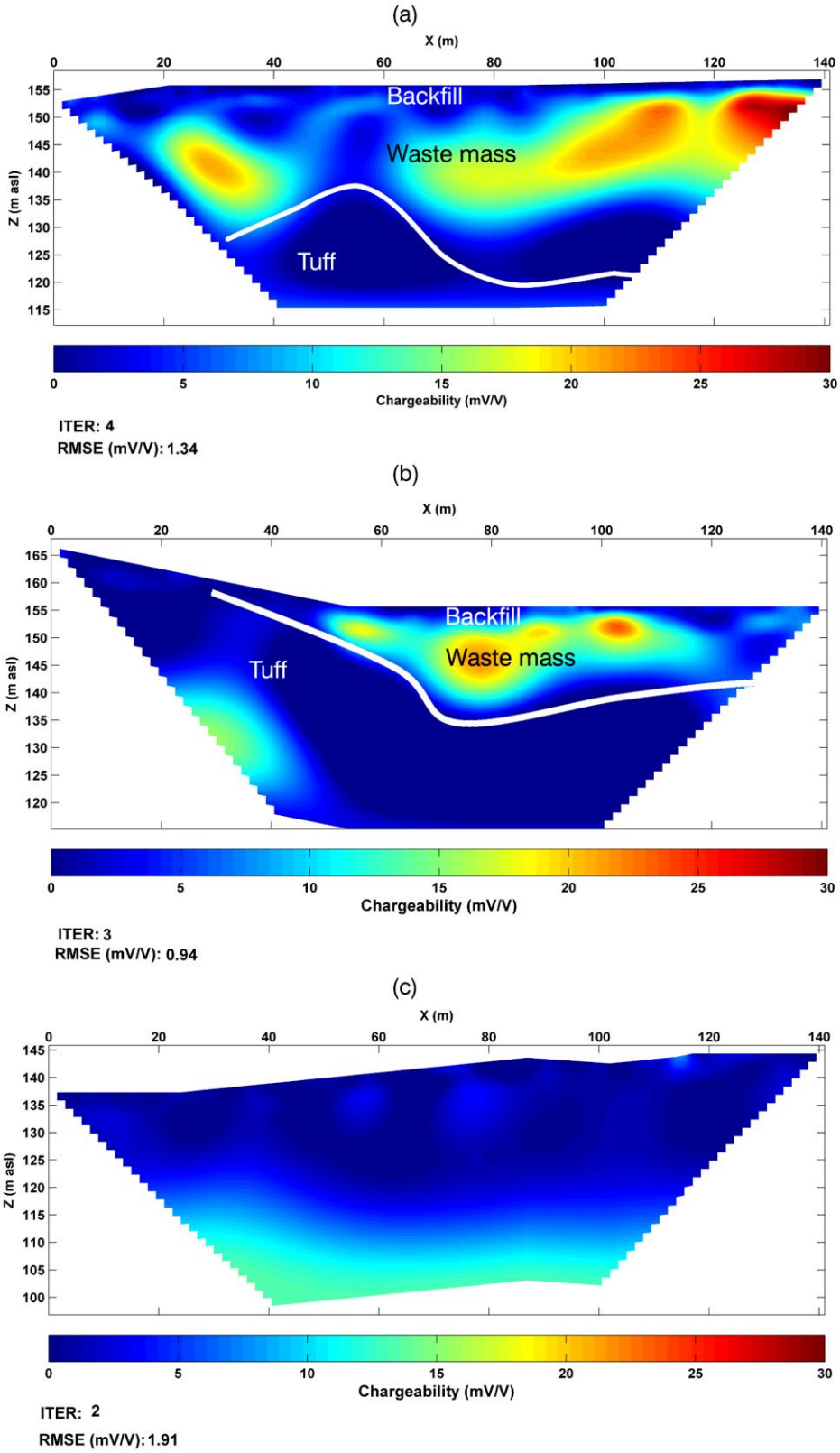

606

607 Figure 6. Chargeability inverted models of ERT/IP L1 (a), L2 (b) and L3 (c) lines for the RW01
608 site. The direction of the line and the position of the first electrode are shown in Fig. 3. The white
609 lines indicate the interface between waste mass and tuff.

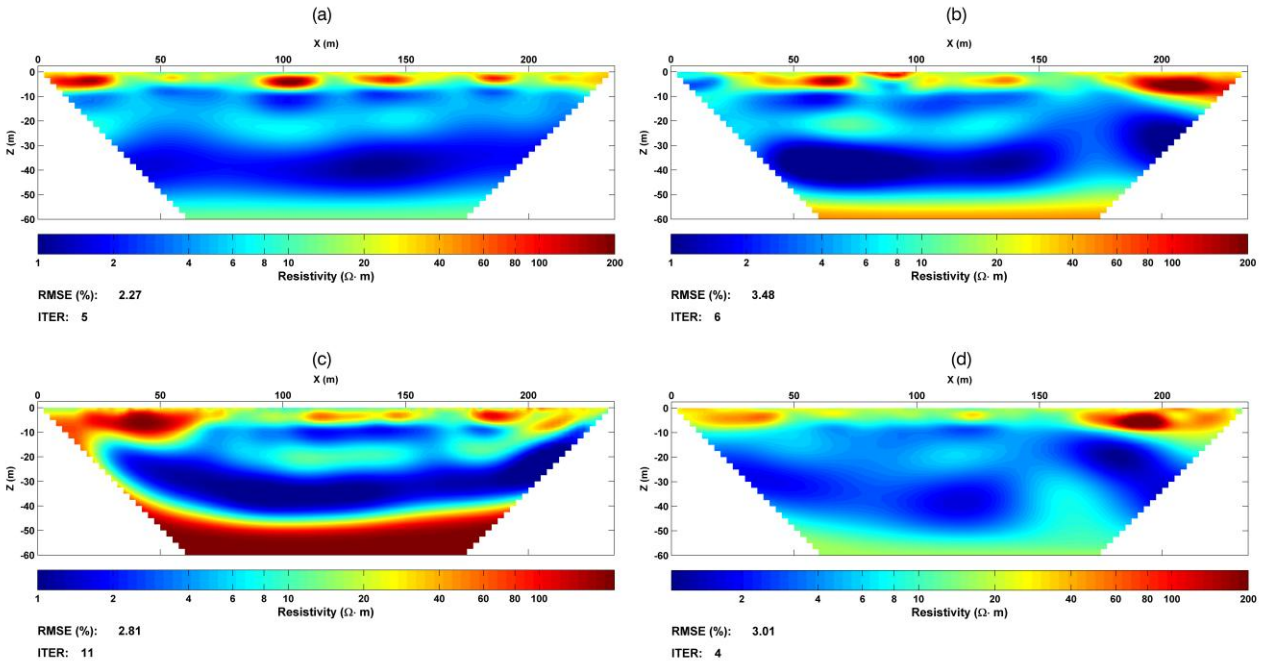

610

611 Figure 7. Resistivity inverted models of ERT/IP L1 (a), L2 (b), L3 (c) and L4 (d) lines for the
612 RW02 site. The direction of the line and the position of the first electrode are shown in Fig. 4.

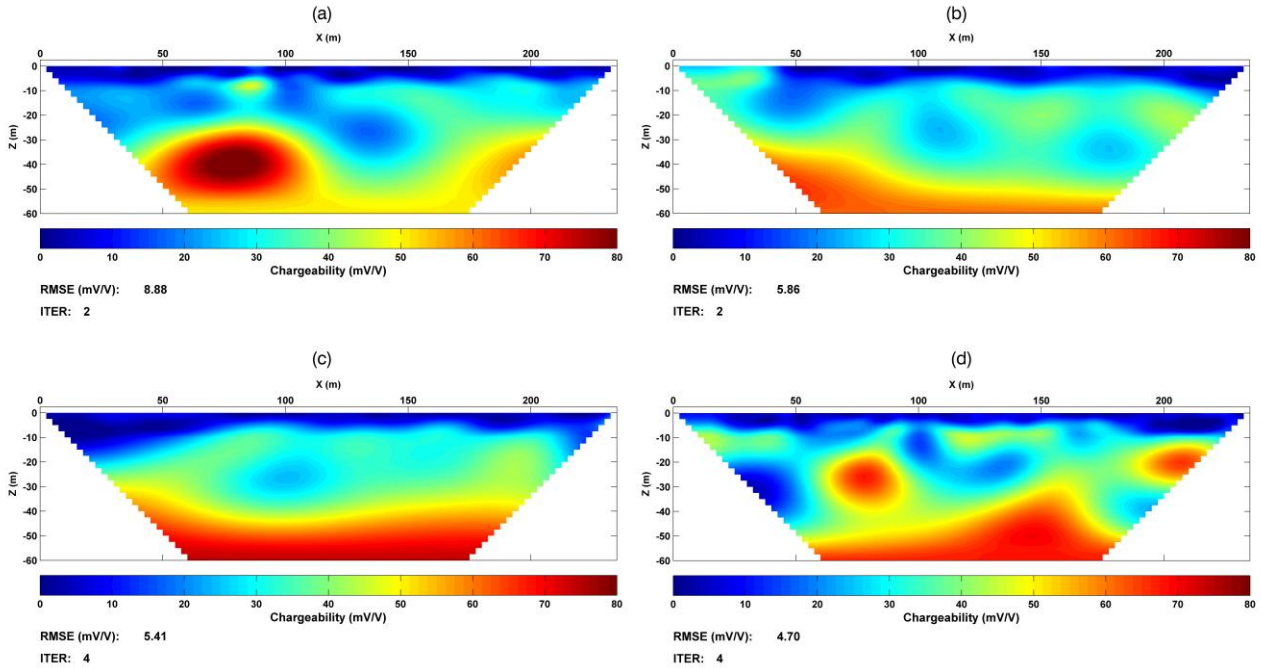

613

614 Figure 8. Chargeability inverted models of ERT/IP L1 (a), L2 (b) , L3 (c) and L4 (d) lines for the
615 RW02 site. The direction of the line and the position of the first electrode are shown in Fig. 4.

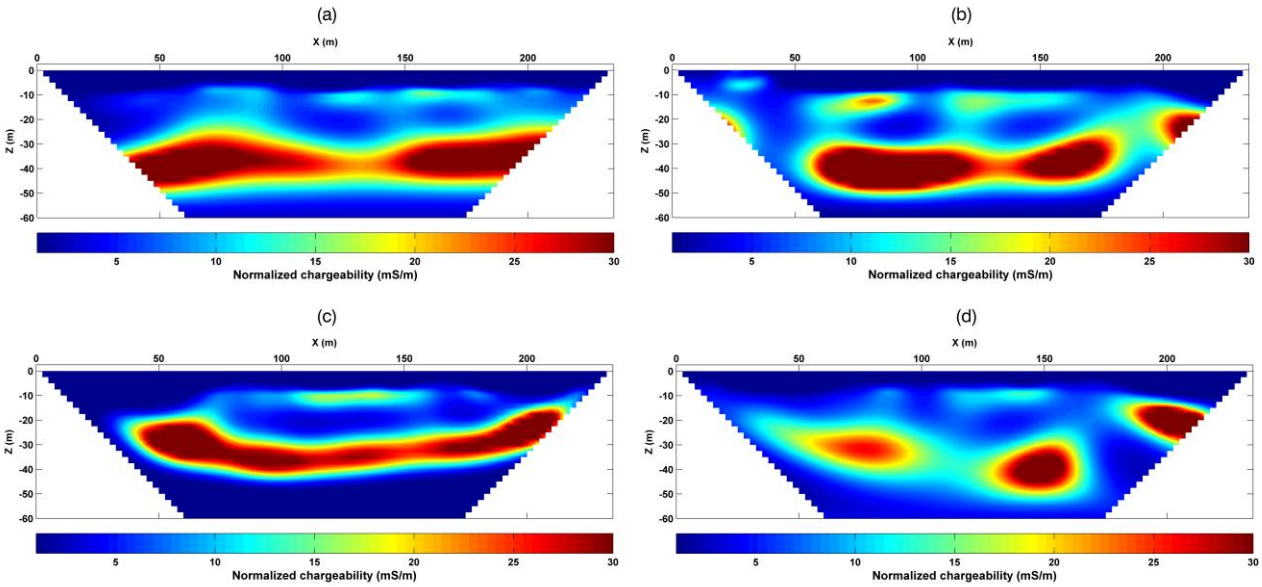

616

617 Figure 9. Normalized chargeability models of L1 (a), L2 (b) , L3 (c) and L4 (d) lines for the RW02
618 site.

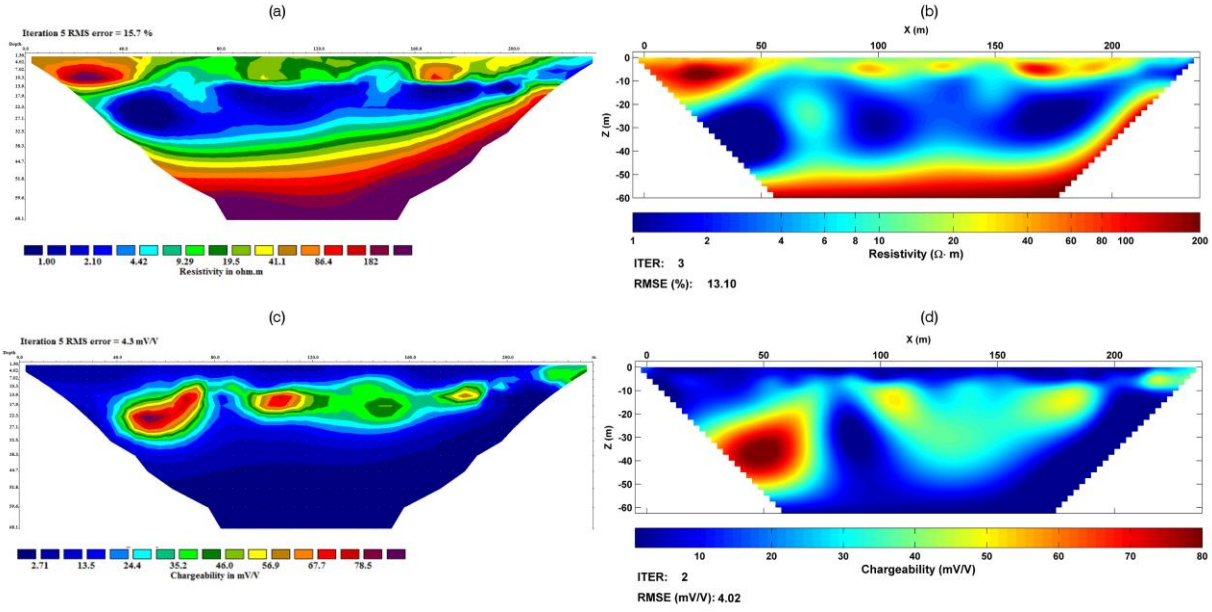

619

620 Figure 10. Resistivity and chargeability inverted models of L3 line for the RW02 using a standard
621 inversion procedure, performed with RES2DINV (a, c) and VEMI (b, d).

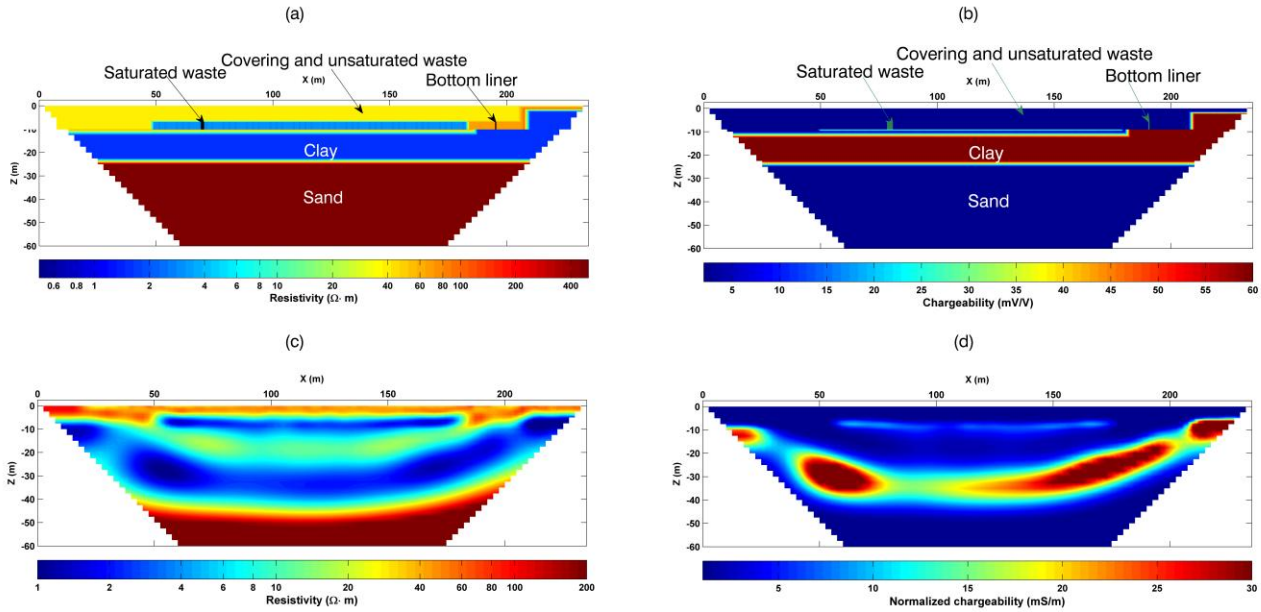

622

623 Figure 11. Landfill model reconstructed using the procedure described in Fig. 2 for the L3 line of
624 RW02. Final landfill model for resistivity (a) and chargeability (b); inverted model at last iteration
625 from synthetic data for resistivity (c) and chargeability (d) to be compared with the inverted model
626 from field data shown in Fig. 7c and 9c.

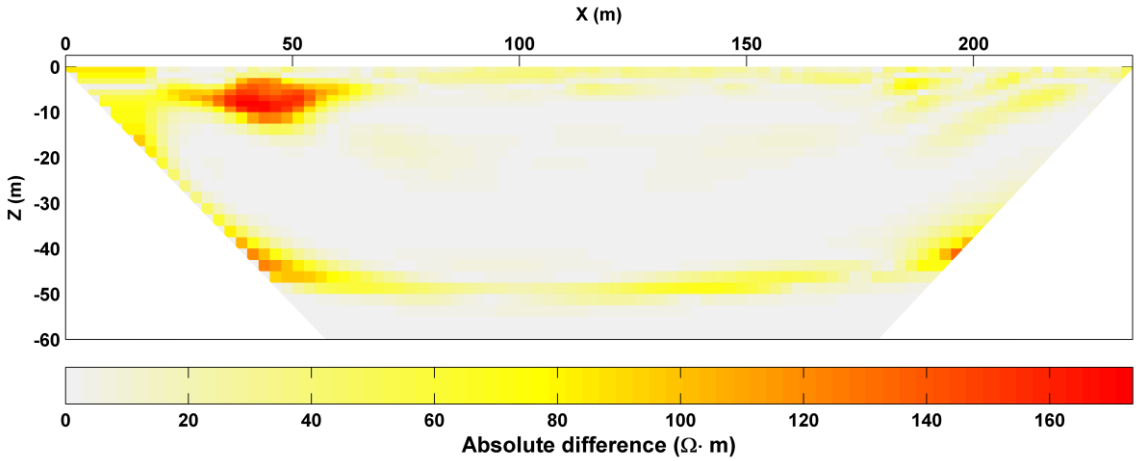

627

628 Figure 12. Absolute differences between inverted models from synthetic and field data for the L3
629 line of RW02.

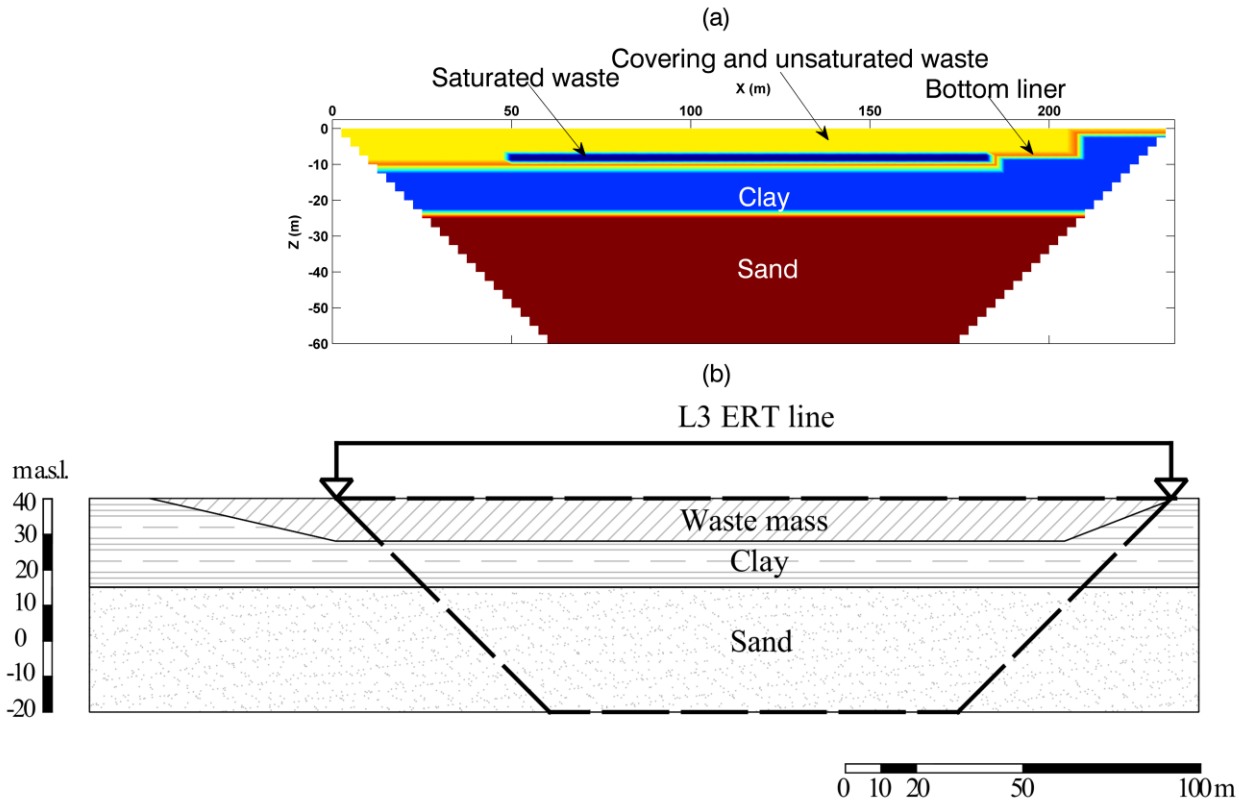

630

631 Figure 13. Comparison between the landfill model obtained for the L3 line (a) and the A-A' section
632 from the construction plans indicated in Fig. 4 (b).

633